Lift Force Analysis in a Controlled - PM LMS Maglev Carrier

K. Yoshida, E. Zen and H. Inoguchi, S. Sonoda, T. Nakao
Kyushu University, Japan Yaskawa Electric MFG. Co. Ltd., Japan

Abstract

The lift force in the controlled permanent-magnet (PM) linear synchronous motor (LSM) Maglev carrier is theoretically evaluated by using the analytical formulas previously proposed by one of the authors and numerical finite-element method (FEM). The proposed theory and the FEM analysis are verified from comparing the calculated results with measured values in the experimental carrier designed on a basis of our analytical formulas.

Controlled-PM LSM Maglev carrier

A long-stator type of LSM with controlled-PM excitation has the integrated functions of LSM propulsion and attractive-mode levitation. Modern PMs with high energy products, such as SmCo or NdFeB material, are applied for basic

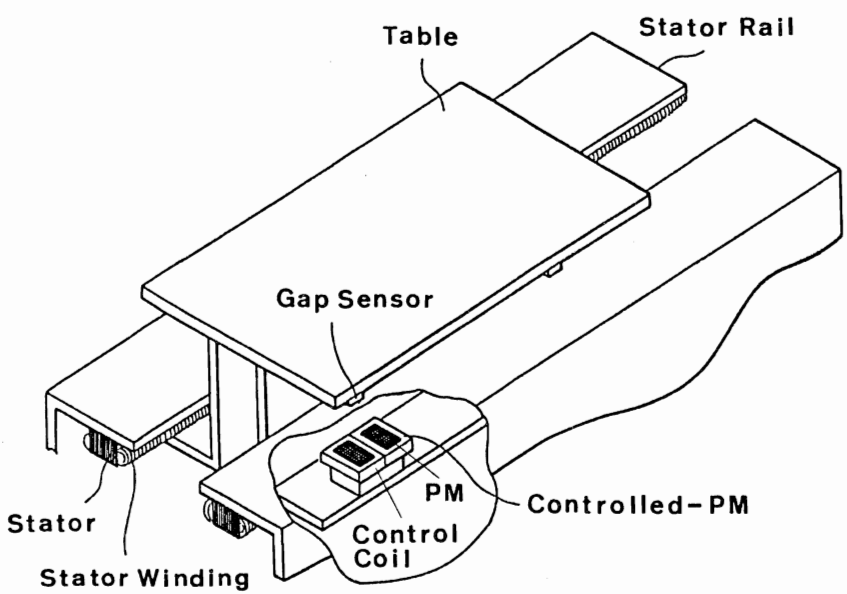

Fig. 1 Configuration of a controlled-PM LSM Maglev carrier

excitation. This machine can be used as contactless actuators or carrier for factory automation (FA) and office automation (OA).

Figure 1 shows configuration of a controlled-$SmCo_5$PM LSM Maglev carrier which has a 2-pole controlled-PM at each of the corners. The experimental carrier is studied here theoretically as well as experimentally.

A 2-pole LSM with controlled-PM excitation shown in Fig. 2 is theoretically treated using an analytical method and numerical FEM in the following.

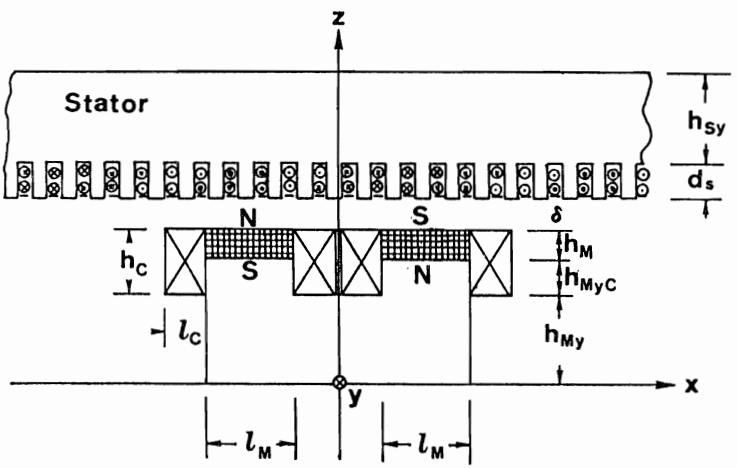

Fig. 2 Cross-section of 2-pole LSM with controlled-PM excitation

Analytical Approach

The translator in Fig. 3 is made of an array of PMs with alternating poarity fixed on a magnet yoke and the control coils wound directly around them. The field analysis of the machine is carried out analytically using a simple PM model [1], which is available for SmCo and NdFeB magnets. The PM modelling is based on the conception of an equivalent non-magnetic layer region which has an impressed volume-current density equivalent to the coercive force and geometries of PM. An impressed volume-current density of the control coils is superposed to that of the PMs in the non-magnetic layer model. The boundary-value field problem is solved analytically using the transfer-matrix method [2]. The formulas for thrust and lift forces are simultaneously derived in the analytical form [3].

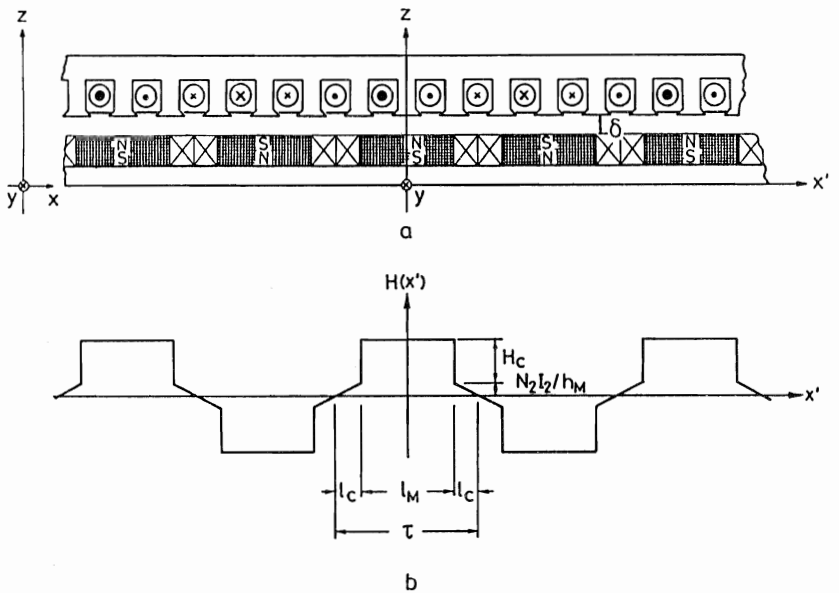

Fig. 3 (a) Cross-section of the LSM with many controlled-PMs mounted directly on magnet yoke

(b) Distribution of the resultant MMF per unit length along the PM height

The lift force consists of three components. The first one is an attractive force of the controlled-PMs attracting magnetically the stator laminated iron. This is the main levitation force and is given as follws :

$$F_{zM}(I_2,\delta_e) = H_c^2 \sum_{n=1,\ 3,\ldots} K_{zMn}(\delta_e)\left(1 + \frac{1}{\pi}\frac{N_2 I_2}{h_M H_c}\frac{\tau}{\ell_C} n \cot k_n \frac{\ell_M}{2}\right)^2 \qquad (1)$$

$$K_{zMn}(\delta_e) = \frac{16}{\pi^2}\mu_0 pb\tau \frac{1}{n^2}\sin^2 k_n\frac{\ell_M}{2}\,\frac{\sinh^2 k_n\frac{h_M}{2}\cosh^2 k_n\left(\frac{h_M}{2}+h'_{Myn}\right)}{\sinh^2 k_n(\delta_e + h_M + h'_{Myn} + h'_{Syn})} \qquad (2)$$

where

$$\tanh k_n h'_i = \frac{\mu_0}{\mu_i}\,\frac{\dfrac{\mu_i}{\mu_0}\dfrac{|k_n|}{k_n} + \tanh k_n h_i}{1 + \dfrac{\mu_i}{\mu_0}\dfrac{|k_n|}{k_n}\tanh k_n h_i} \qquad i = My,\ Sy \qquad (3)$$

$$\delta_e = k_c \delta \quad ; \quad k_c = \text{Carter's coefficient} \tag{4}$$

When Eqs.(1) - (4) are applied to the calculation of lift force in the 2-pole machine in Fig.2, attention is paied to the difference between Figs. 2 and 3. The longitudinal end effect due to leakage flux and the effect of iron saliency between PM and magnet yoke can not be taken into account in the analytical model in Fig. 3.

Numerical Analysis via FEM

Numerical analysis method is suitable for mathematical model of some complex geometry as shown in Fig. 2. FEM is used, via which the non-linearity of magnet and stator yokes are taken into considerations.
When PM is magnetized constantly along the PM height with a magnitude of coercive force H_c, the equivalent volume-current density is given by [4]

$$i_M(\ell_C, z_0) = H_c \delta(\ell_C, z_0) \ , \quad i_M(\ell_C+\ell_M, z_0) = - H_c \delta(\ell_C+\ell_M, z_0)$$
$$(h_{My}+h_{MyC} \leq z_0 \leq h_{My}+h_{MyC}+h_M) \tag{5}$$

where $\delta(\ell_C, z_0)$ and $\delta(\ell_C + \ell_M, z_0)$ are δ function.
Tnis Eq.(5) means that PM can be replaced by equivalent current sheet on the side surface of the PM. Ampere-turns $H_c h_M$ and $- H_c h_M$ are equally distributed at the nodes of each side surface of the PM.
Current-carrying control coils are treated similarly by distributing equally ampere-turns $N_2 I_2$ or $- N_2 I_2$ at the nodes in each cross-section of the control coils.

Numerical Calculations and Experiments

The flux pattern, and the space distribution of the x-and z-components of airgap flux density and attractive force are calculated using FEM and are shown in Fig. 4. It is found,especially from symmetricity of attractive force per pole with respect to each pole axis, that the end effects are almost negligible. In case of carrier with very small airgap length, airgap flux is concentrated strongly within the magnet length, due to very high coercive force of $SmCo_5$ magnet.

Figures 5 and 6 show a comparison between calculated results from Eqs.(1)-(4) and via FEM and measured values, regarding the stator without slots.

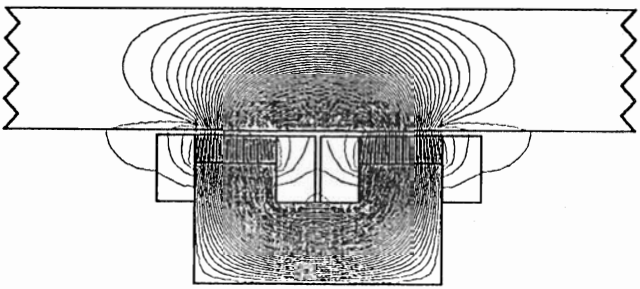

(a) Magnet field contours

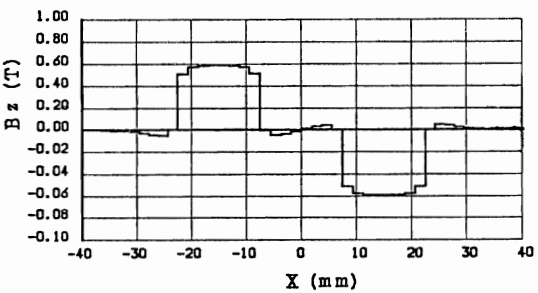

(b) The z-component of the airgap flux density at the stator surface

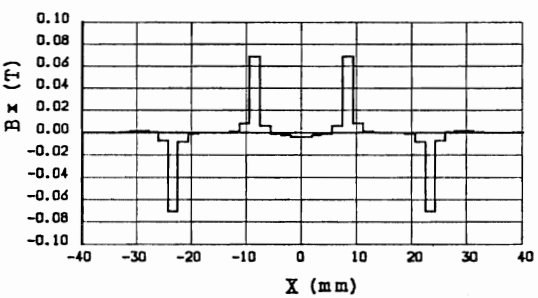

(c) The x-component of the airgap flux density at the stator surface

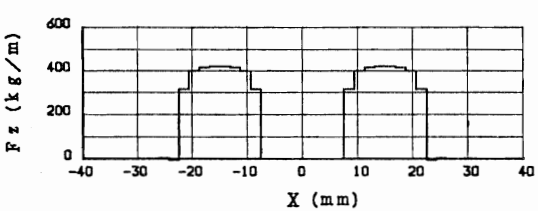

(d) The attractive force at the stator surface

Fig. 4 Spacae distribution of parameters at δ = 1mm
under control current I_2=-15A

The measured values are obtained by adding the four values measured independently for each controlled-PM of carrier. Figures 7 and 8 show a comparison between the calculated results and measured values, regarding the stator with slots. The measured values are obtained when the experimental carrier is levitated stationary by the controller. In Fig. 7 the control current I_2 is controlled to be almost zero, by regulating sensitively the airgap length of the four controlled-PM. The net weight of the carrier is about 26kg, which corresponds to the airgap length of about 3.5mm as shown in Fig. 7.

The theoretical values are somewhat larger than the experimental ones. But they generally show a good agreement. Though FEM treats more exact model, it has tendency to overestimate the lift force. Analytical method explains more precisely the experimental results. The analytical formulas propsed are verified experimentally and theoretically to be effective in the design of 2-pole controlled-PM LSM with iron saliency, which is used for Maglev carrier.

Acknowledgements

Thanks are due to Mr. N. Teshima for carrying out the lift force measurements and to Mr. H. Kawanami for preparation of this paper.

References

[1] Yoshida, K. and Weh, H. : A Method of Modeling Permanent Magnets for Analytical Approach to Electrical Machinery, Archiv f. Elektrotechnik, No. 4 Vol. 68 (1985) 229-239

[2] Yoshida, K. : New Transfer-Matrix Theory of Linear Induction Machines, taking into account Longitudinal and Transverse Ferromagnetic End effects, IEE Proc. 128 Pt. B (1981) 225-236

[3] Yoshida, K. and Weh, H : Analytical Approach to Linear Synchronous Motors Excited Using Flat Type Controlled Permanent-Magnets, Proc. of Int. Conf. on Elect. Machines, Part 1 Lausanne Spt. 1984

[4] Yoshida, K and Zen, E. : Theoretical and Experimental Study of Lift Force in Small Type LSM with Controlled-PM Excitation, Report-88-18 of the Studying Committee on Rotating Machinery

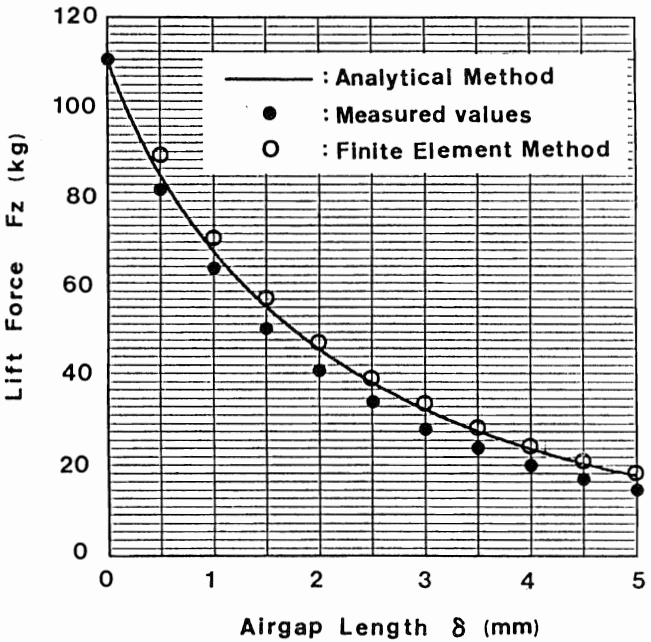

Fig. 5 Lift force vs. airgap length characteristics for slotless stator-laminated-iron under the control current $I_2 = 0$

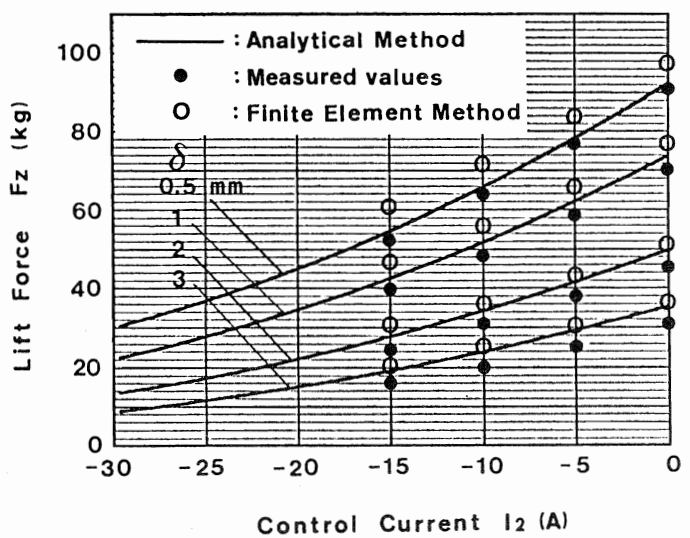

Fig. 6 Lift force vs. control current characteristics for slotless stator-laminated-iron under the airgap length δ = 0.5mm, 1mm, 2mm and 3mm

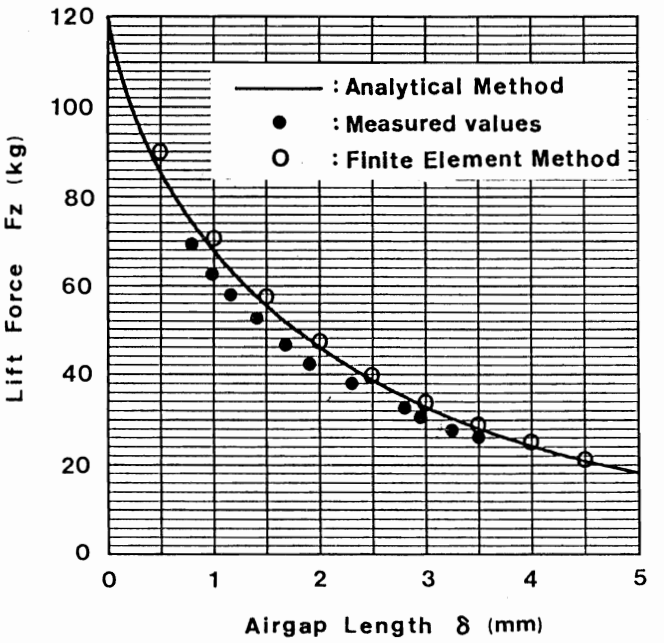

Fig. 7 Lift force vs. airgap length characteristics for slotted stator-laminated-iron under the control current $I_2 = 0$

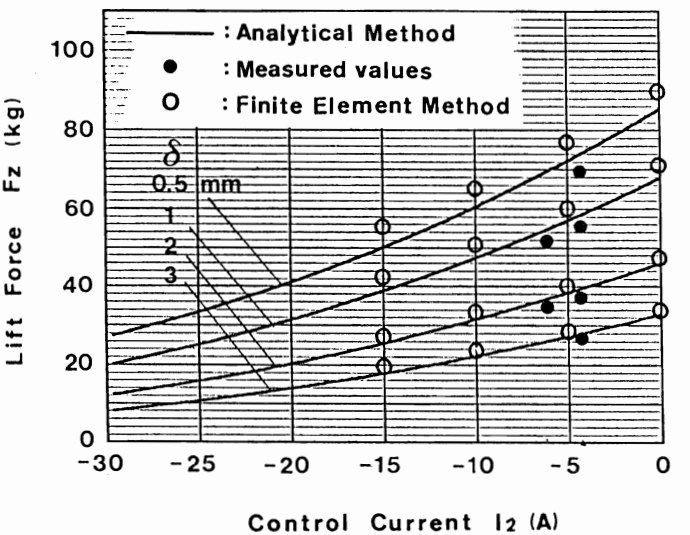

Fig. 8 Lift force vs. control current characteristics for slotted stator-laminated-iron under the airgap length δ = 0.5mm, 1mm, 2mm and 3mm